Biosensors and Bioelectronics 61 (2014) 298–305

Contents lists available at ScienceDirect

Biosensors and Bioelectronics

journal homepage: www.elsevier.com/locate/bios

Single-cell trapping and selective treatment via co-flow within a microfluidic platform

A. Benavente-Babace [a,b,*], D. Gallego-Pérez [c], D.J. Hansford [c], S. Arana [a,b], E. Pérez-Lorenzo [a,b], M. Mujika [a,b]

[a] CEIT-IK4 and Tecnun, University of Navarra, Manuel de Lardizabal 15, 20018 San Sebastián, Spain
[b] CIC microGUNE, Goiru Kalea 9, 20500 Arrasate-Mondragon, Spain
[c] Department of Biomedical Engineering, The Ohio State University, Columbus, Ohio 43210, USA

ARTICLE INFO

Article history:
Received 17 January 2014
Received in revised form
13 May 2014
Accepted 15 May 2014
Available online 24 May 2014

Keywords:
Microfluidic chip
Single-cell analysis
Laminar co-flow
Toxicity assay
Cell-based biosensor

ABSTRACT

Lab on a chip (LOC) systems provide interesting and low-cost solutions for key studies and applications in the biomedical field. Along with microfluidics, these microdevices make single-cell manipulation possible with high spatial and temporal resolution. In this work we have designed, fabricated and characterized a versatile and inexpensive microfluidic platform for on-chip selective single-cell trapping and treatment using laminar co-flow. The combination of co-existing laminar flow manipulation and hydrodynamic single-cell trapping for selective treatment offers a cost-effective solution for studying the effect of novel drugs on single-cells. The operation of the whole system is experimentally simple, highly adaptable and requires no specific equipment. As a proof of concept, a cytotoxicity study of ethanol in isolated hepatocytes is presented. The developed microfluidic platform controlled by means of co-flow is an attractive and multipurpose solution for the study of new substances of high interest in cell biology research. In addition, this platform will pave the way for the study of cell behavior under dynamic and controllable fluidic conditions providing information at the individual cell level. Thus, this analysis device could also hold a great potential to easily use the trapped cells as sensing elements expanding its functionalities as a cell-based biosensor with single-cell resolution.

1. Introduction

Cell handling is essential for research and application development in clinical diagnostics. However, in numerous biological assays thousands of cells are cultured without considering that the interaction among them may interfere in the resulting data. Nowadays it is well known that individual cells, even those with identical appearance, differ from each other in many characteristics, such as the critical amount of a metabolite or the specific genetic expression (Graf and Stadtfeld, 2008; Walling and Shepard, 2011). These disparities make individual cells have different responses to equal stimulus in the same conditions. This is critical in their function and viability and the obtained average results may lead to ambiguous information. Studying cell populations at single cell level without the influence of the neighboring cells opens new opportunities for more personalized diagnostics and drug discovery. However, an accurate individual cell manipulation is not straightforward. Therefore, developing strategies able to control each cell individually constitutes a hot topic in the field. In this light, microfluidics emerges as a powerful alternative. Particularly, microfluidics is a multidisciplinary field that studies the dynamic of fluids confined in the micro-scale range.

In the last twenty years, the inherent capacity of microfluidics for handling small sample volumes and molecules with high control has made it the preferred alternative of researchers to overcome most of the drawbacks of traditional culture assays. Lab-on-a-chip devices, based on micro-technologies, allow splitting (Jeon et al., 2000), mixing (Stroock et al., 2002) and analyzing (Skommer et al., 2012; Toner and Irimia, 2005; Velve-Casquillas et al., 2010) a single drop sample (urine, blood, etc.) in a high throughput manner and with minimized samples, reagents and waste thanks to their length scale. Furthermore, all these advantages, inherent to miniaturization, are combined with the use of cheap polymeric materials for their fabrication, which translates to a great reduction of overall costs compared to their macro-scale counterparts (Bange et al., 2005; Chou et al., 2013; Sia and Whitesides, 2003; Weigl et al., 2008)

A great amount of appealing studies can be performed with high spatial and temporal resolution, being of great interest those involving the manipulation of single cells (Zare and Kim, 2010). This control is mostly possible because, under these micro-scale conditions where viscous effects dominate over inertial forces, the

* Corresponding author. Tel.: +34 943 212 800; fax: +34 943 213 076.
E-mail address: abenavente@ceit.es (A. Benavente-Babace).

http://dx.doi.org/10.1016/j.bios.2014.05.036
0956-5663/

flow is totally laminar meaning that multiple liquid streams can flow side-by-side in a predictable manner and without turbulent mixing (Kovacs, 1998).

This manipulation of two or more fluids at a time is known as co-flow phenomena. The straightforward example is the use of several fluids as 'virtual walls', called sheath flows, for steering the main flow. This technique is commonly known as hydrodynamic focusing and has been widely used for improved flow cytometry (Bhagat et al., 2010; Hur et al., 2010; Joo et al., 2010; Oakey et al., 2010).

Beyond these works, laminar co-flow has been used for several applications. For instance, Parra-Cabrera et al. (2012) carried out an on-chip selective surface functionalization procedure for biosensors using laminar co-flow. In the same way, Takayama et al. (1999) patterned cells or even treated just parts of them and/or their substrate. This high spatial control and resolution was also exploited by the same group to deliver multiple reagents to selected subcellular microdomains of a single living cell (Takayama et al., 2001). Similarly, Li et al. (2011) developed a technique for studying cell behavior under two or more gene transfections in the same culture thanks to partial transfection of cells using two flows.

Closely related to hydrodynamic focusing, hydrodynamic resistance emerged as one of the most reported techniques for isolating single cells in spatial confinement (Arakawa et al., 2011; Di Carlo and Lee, 2006; Faley et al., 2009; Frimat et al., 2011; Kobel et al., 2010; Rowat et al., 2009; Wu et al., 2008). However, whilst the hydrodynamic focusing takes advantage of the co-flow, the latter does not. Exploiting the cleanness and versatility of the laminar co-flow together with robustness of hydrodynamic based trapping methods could lead to simplified and cost-effective microfluidic platforms for a number of different applications including enhanced cell-based biosensors (Z.H. Wang et al., 2012, T. Wang et al., 2013). However, further efforts are required for combining all the existing functionalities of this kind of systems making use of their potential for single cell studies (Xu et al., 2005).

In this work we merge both methodologies: (1) the use of co-flow phenomena for a broaden functionality of a microfluidic platform and (2) single-cell analysis. Concretely, we develop and characterize a simple and reliable PDMS microfluidic platform for on-chip single cell selective trapping and treatment. The presented study describes the optimum parameters for single-cell trapping and explains the procedure based on the use of laminar flow of multiple parallel liquid streams to selectively treat cells of the same population at individual level. The control of the co-flow is achieved by varying the ratio of the input flows. In order to fully control the occupation of each stream inside the device several characterization curves are obtained both, theoretically and experimentally. Finally, we demonstrate the utility of our novel device for setting the threshold ethanol concentration that is toxic to single cells. The whole system is a potential solution for determining the minimal dosage of different drugs in cancer research providing with quantitative information at single-cell level.

2. Material and methods

2.1. Microdevice design and fabrication

A microfluidic device for single cell analysis was developed as shown in Fig. 1a. As in Benavente-Babace et al. (2013), the polydimethylsiloxane (PDMS) based platform consisted of two inlets and two outlets with a wider section at the middle of the device (the trapping chamber) where the cells are captured and studied under certain given conditions. The dimensions of the chamber were 4 mm long, 500 μm wide and 27 μm high, containing arrays with different sieve-like structures (see inset of Fig. 1b).

The microfluidic device was fabricated using common PDMS replica-molding processes (see Supplementary information, Fig. S2). First, the master was fabricated by conventional UV photolithographic techniques onto a 4″ silicon wafer. After cleaning the wafer in piranha solution (H_2SO_4:H_2O_2/1:1) it was spin-coated with a negative photoresist (SU-8 2025, MicroChem Co.) at 2600 rpm in order to achieve a thickness of 27 μm. Then, the wafer was soft-baked, exposed to the specific photomask, post-baked and developed according to manufacturer instructions. Finally, this master mold was rinsed with isopropanol to clean the residues from the photoresist and dried, concluding with a hard-bake step for 2 min at 150 °C in order to get rid of stress cracks.

A two-part mixture (base:curing agent/10:1) of polydimethylsiloxane (Silastic T4 PDMS, Dow Corning) was then poured and cured at room temperature for 48 h upon the silicon master to produce an optically transparent replica. The silicone replica was disassembled and the inlets and outlets were punched by a needle. Finally, it was bonded to a previously cleaned glass slide by means of 1 min oxygen plasma treatment at 100 W (Femto, Diener Electronic).

A preliminary characterization of the silicon and PDMS microstructures was conducted using optical microscopy and scanning electron microcopy (Hitachi S3000-H). Prior to imaging, the devices were coated with a thin Au/Pd layer to prevent charging.

2.2. Experimental setup

The experimental setup used in the experiments is shown in Supplementary Fig. S3. For fluid insertion or cell loading, one syringe pump per inlet (*eS-pump ESR200P*, NanoNC Co. Ltd. and KDS *SP101i*, WPI Inc.) was used. Both pumps were connected to the microdevice through Tygon tubing (O.D.=2.18 mm and I.D.=0.38 mm, Saint-Gobain Performance Plastics, France) using 1 mL plastic syringes (Becton, Dickinson and Company). The microfluidic platform was placed on an inverted microscope with an incorporated digital camera (Nikon Eclipse TS100 and Nikon D90) in order to monitor and record the experiments.

2.3. Fluid dynamics

The low Reynolds number found within this microfluidic platform fixes an entirely laminar flow. These conditions ensure that mixing occurs only by diffusion, which will depend on the flow rate and on the length of the interface between two fluids. This fluid system has the advantage that it is easily controlled and modeled. The virtual wall between fluids can be displaced as required just by controlling the flow rate ratio at the inlets (Fig. 2). Based on this concept, this microdevice can be used to treat or functionalize simultaneously and under the same conditions specific parts of the chamber with two different solutions. In order to precisely control this moving interface, or the chamber occupation by each fluid, the fluid dynamics through the device was characterized experimentally and the main results were contrasted theoretically.

For the characterization of flow, an un-dyed phosphate-buffered saline solution and a blue-dyed one (DPBS, Lonza) were used to optically locate the interface between them. Different concentrations of PBS and ethanol (Panreac) mixture were also analyzed to find out if solutions with different density and viscosity would affect the behavior of the dynamic interface.

Several ratios between the two input flows (Q_{main} and Q_{lat}) were defined in order to fully control the chamber occupation. Specifically, the following ratios were studied: Q_{main}/Q_{lat} (or Q_{lat}/Q_{main})=1, 1.5, 2, 4,

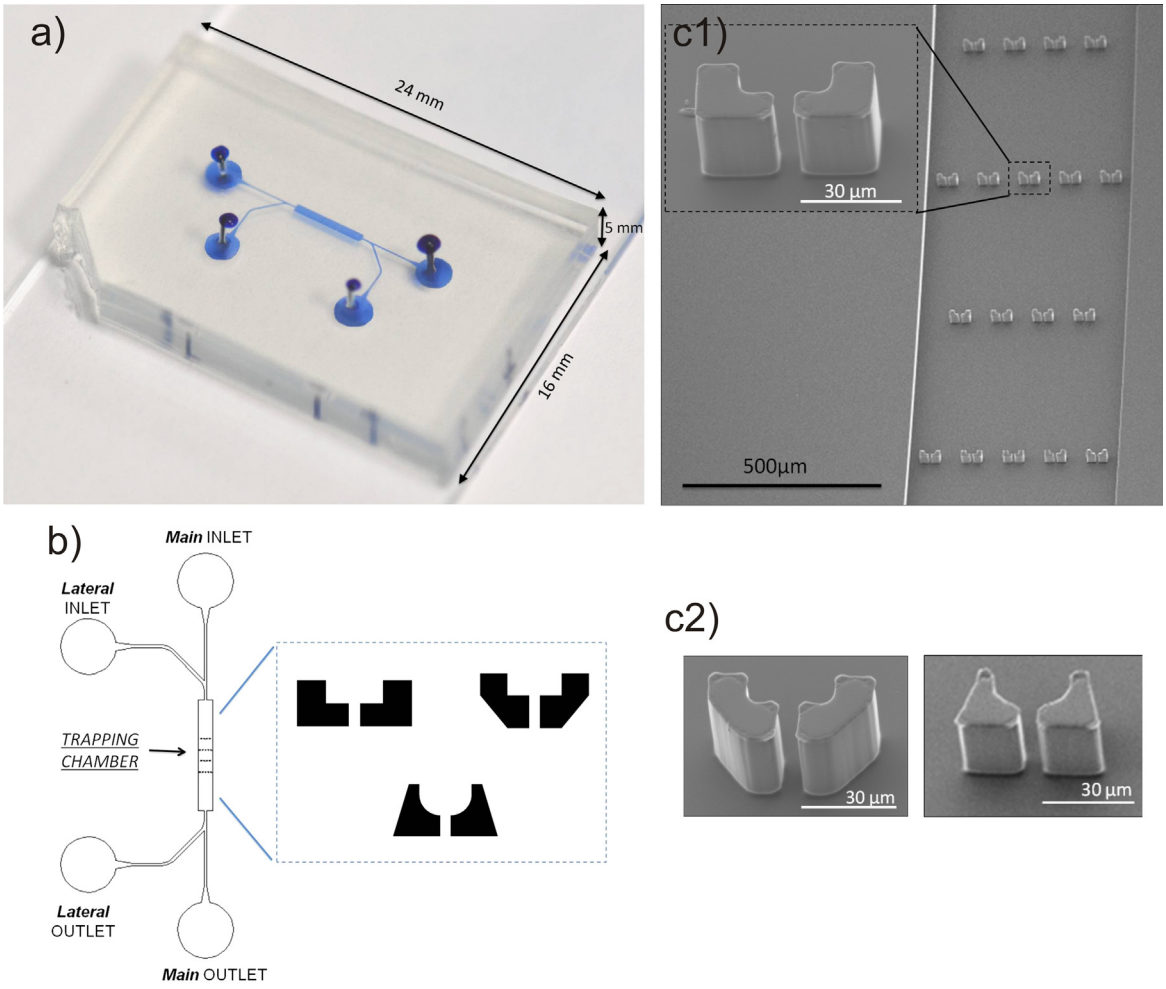

Fig. 1. (a) Picture of the fabricated device. (b) Schematic of the microfluidic platform. The inset shows the three different designs of the sieve-like structures for trapping cells. (c) SEM micrograph of the PDMS device. (c1) Trapping chamber. Inset: sieve-like structure. (c2) Different geometries of the sieve-like structures.

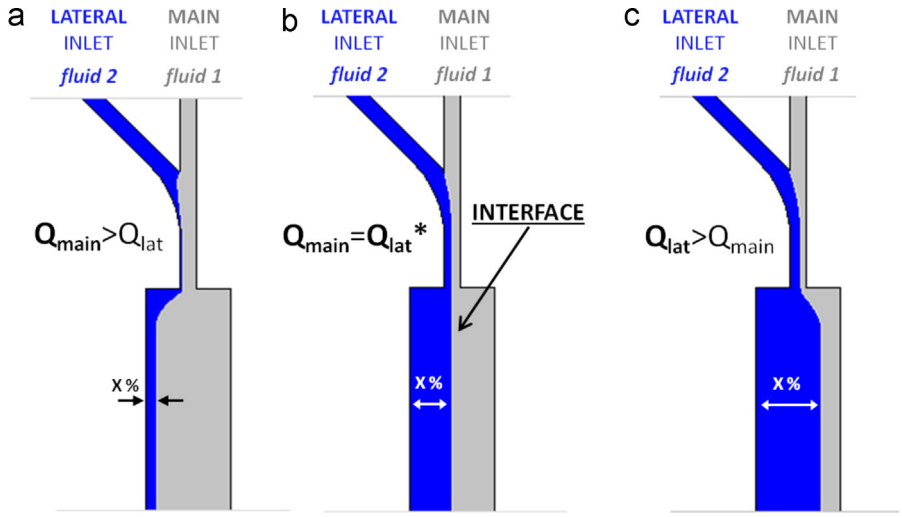

Fig. 2. Standard examples of some possible flow rate ratio configurations for different chamber occupancy of the fluids. *When both solutions have the same physical properties, for a flow rate ratio of 1, the chamber occupation will be 50% for each fluid.

5, 6, 8, 10 and 12. As these ratios can be achieved within different flow rate ranges, low (.1 μL/min < Q < 1 μL/min), medium (1 μL/min- < Q < 10 μL/min) and high (10 μL/min < Q < 25 μL/min) flow rate intervals were defined and analyzed.

Computational fluid dynamic (CFD) simulations, based on Navier–Stokes equations, were performed in COMSOL (Comsol Multiphysics 4.2a, Sweden) to analyze the co-flow behavior through the microfluidic network. Different input flow ratios were

evaluated in order to steer the moving interface through the whole chamber validating the experimental characterization.

2.4. Cell culture and device operation

Mouse hepatocytes (AML12 cell line, ATCC) were maintained in Dulbecco's modified Eagle's medium with Nutrient Mixture F-12 (D-MEM/F12, Gibco) containing Glutamax, 10% fetal bovine serum (FBS) and 1% of antibiotics. They were incubated in a humid atmosphere at 37 °C with 5% CO_2.

Prior to its use with cells, the device and the tubing were sterilized with 70% ethanol. Then, the system was filled with phosphate buffer saline solution through the lateral inlet (see Fig. 1b) ascertaining that any bubble inside the device was removed. Afterwards, cell suspensions were loaded in a 1 mL syringe and flowed into the device through the main inlet. The flow rate ratio between both inlets was adjusted in order to control the specific line of traps to be filled. Once the arrays of traps were filled with cells, the syringe pump governing the main inlet was stopped and the syringe with individual cells was replaced by another one with fresh media. At this stage, both inlets could be used for driving any other fluid depending on the following assay to be made, i.e. trypan blue for checking cell viability or a specific drug for testing it.

2.5. Cytotoxicity assay

As a proof of concept, the effect of different ethanol concentrations on mouse hepatocytes was tested and the threshold ethanol dosage that is toxic to single cells was determined. The ethanol concentrations used were 0% (as a control), 10%, 15%, 20%, 25%, 30%, 40%, 50%. Trypan blue (Gibco, Life Technologies) exclusion test was used for quantifying the cytotoxic effect of ethanol. Note here that we are considering cytotoxicity in its extended meaning; understanding that ethanol is toxic to cells not just because it may active the apoptotic mechanisms that in the end will cause cell death, but also because cells exposed to ethanol may undergo necrosis, in which they lose membrane integrity and die rapidly as a result of cell lysis.

At least three experiments were run for each ethanol concentration. Once all the traps were filled with single cells and the untrapped cells were removed, .4% trypan blue was injected through the lateral inlet to check the captured cell viability prior to the treatment. Then, the specific ethanol dosage was perfused through the main inlet and the correct flow rate ratio for both inlets was fixed for treating only the selected single cells while the rest remained untreated as a control. Cell viability was checked every minute during the first 5 min and then every 5 min until all the seized and treated cells were dead. Note that cells were never exposed to trypan blue for more than 60 min to avoid misleading data from the own toxicity of this substance.

2.6. Image analysis

In order to quantify the occupation of the chamber by each fluid a custom-made MATLAB (The MathWorks, Inc.) script for automation of these measurements was implemented. Specifically, the program measures the distance from the left wall of the trapping chamber to the interface, giving the percentage [%] of the deviation of the fluid 2 (the one that enters from the lateral inlet) over the entire width of the chamber (Fig. 2). Note that, all the images were taken in the middle part of the chamber where the trapping sieve-like structures are placed. This standalone interface detection provides accurate, repeatable and unbiased results. Further details about the operation and adaptability of this developed program can be found in the Supplementary information.

2.7. Statistical analysis

All statistical analyses as well as the graphical representations were carried out using MATLAB. Data are presented here through the corresponding mean values.

The experimental fluctuations observed when identifying the flow rate ratios leading to a chamber occupation of a 50% are illustrated by means of error bars, representing one standard deviation above and below the mean. Assuming that the experimental data are normally distributed these intervals constraint about the 95% of the points.

The exposure time until cell death studied in the cytotoxicity analysis is represented by means of boxplots. The box extends from the first quartile to the third quartile values with an additional horizontal line that represents the median. The whiskers are vertical lines that go from each end of the box till the most extreme data value within 1.5 times the interquartile range. In this analysis 142 time points were considered.

3. Results and discussion

3.1. Fabricated microfluidic platform

SEM micrographs (Fig. 1c) confirmed that all the features were accurately reproduced from the master molds. The microfluidic system was 27 ± 1 μm high. The trapping arrays within the main chamber of the device consisted of four rows containing pocket-like structures with three different geometries, but all having a small aperture of 6 ± 1 μm (Fig. 1d). With smaller gaps the fraction of fluid streamlines going through the traps was too small that the cells dodged these structures. However, with gaps bigger than 6 ± 1 μm cells squeezed and slid from the trap. All the dimensions were tailored for optimizing the device for a cell diameter of 15–20 μm. The tested microdevices had a total of 14–18 traps; however the whole chamber could be easily enlarged increasing the amount of these structures without disturbing any other parameter and enabling high throughput analyses.

We found that for an optimal definition of the microtraps the developing time during mold fabrication was 3–4 min longer than the standard established by the manufacturer.

3.2. Fluid dynamics characterization for selective fluid control within the chamber

The interaction between PBS–PBS and PBS–ethanol [*X*%] was studied in order to characterize the fluid dynamics inside the microfluidic system. Ten ratios at different flow rate ranges were analyzed between two input flows in order to fully control the chamber occupation. This system allowed to have two different fluids simultaneously covering separated parts of the device analysis site (Fig. 3a). Noteworthy differences were observed depending on the flow rate or when enclosing two fluids with different physical properties such as viscosity or density. Experimental conditions carried out in the frame of this study were also reproduced by Computational Fluid Dynamics simulations. Obtained results showed a good agreement with the experimental data, as illustrated in Fig. 3b.

3.2.1. Chamber occupation

Fig. 3b shows the flow rate ratios needed to accurately control the occupation of the chamber. This study was conducted in the same way for both: flow rates of fluid 1 greater than those of fluid

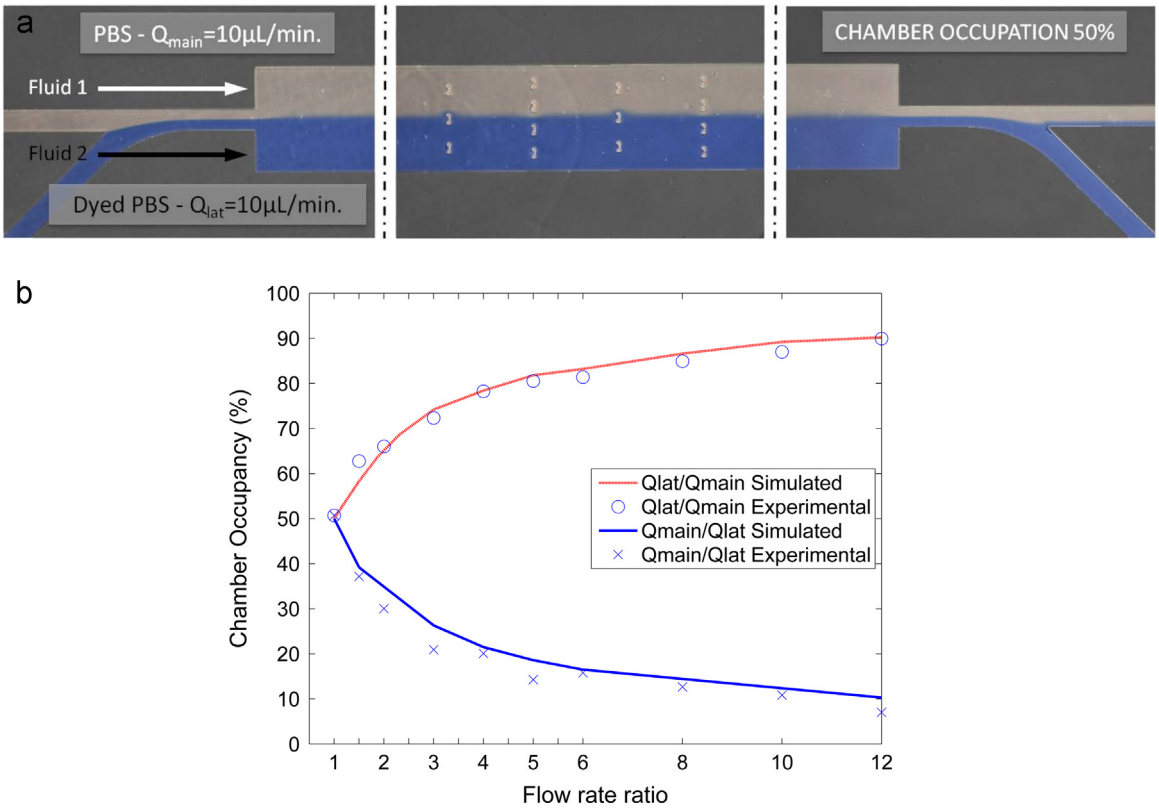

Fig. 3. Theoretical and experimental results. (a) Optical microscopy image showing the laminar flow within the device. (b) Chamber occupation obtained for different flow rate ratios between inlets. Dots and stars represent the median of all obtained values of the taken pictures from the performed experiments. Continuous and dotted lines show the simulated results of the chamber occupation percentage.

2 ($Q_{main}/Q_{lat} > 1$) and inversely ($Q_{lat}/Q_{main} > 1$) (see Fig. 3b). Data confirm that experimental and simulated results are in good agreement. The relationship between chamber occupation and inlets flow rate ratio shows two distinguishable areas. In particular an asymptotic behavior is observed in extreme chamber occupations whilst an exponential growth occurs where both flow rates are similar, namely the ratio is close to one ($Q_{main} \approx Q_{lat}$). Therefore, a chamber occupation above 90% demands ratios in the order of 20. These ratios, however, require extreme flow rate ratios which could lead to negative consequences in the study under consideration such as bad performance of the syringe pumps or forced diffusion of one of the fluids. Normally, when the chamber occupation has to be close to 100%, one of the syringe pumps should be halted.

Another interesting insight obtained from the figures above is that the asymmetry of the inlets does not affect the flow. In other words, the length of the channel before the chamber allows the flow to become fully developed. For instance, note from Fig. 3 that when the same flow is introduced through both inlets, the chamber occupations is precisely close to the 50%, highlighting that the interface position indeed is not dramatically affected by the asymmetry of the inlets. This effect is clearly seen in the symmetry with respect to 'Flow rate ratio' axis kept by Q_{main}/Q_{lat} and Q_{lat}/Q_{main} curves (Fig. 3b). Remember that, when working with ratios, it is possible to get the same chamber occupation using different flow rates.

3.2.2. Flow rates

The magnitude of the flow rates under consideration represents a parameter of utmost importance. For instance, results obtained using low flow rates, namely those below 1 μL/min, turn out to be less consistent than higher ones. This is mainly caused by experimental artifacts, as it is that, the optimal operation range of the pumps does not correspond to these flow rates. In addition, flow rates below 1 μL/min may not be of interest since they lead to higher diffusion. As a consequence, an accurate flow control may not be possible since both fluids are mixed in a larger region due to this phenomenon, as shown in Supplementary Fig. S4.

3.2.3. Fluid properties

When two different fluids (or fluids with different physical properties) are introduced within the device, an occupation of 50% is not achieved even when the flow rate ratio is equal to one. This is mainly because both fluids have different biophysical properties such as density or viscosity, as noted in the case of ethanol and dyed PBS in Supplementary Fig. S4. Ethanol at different concentrations, both diluted in PBS and water, was studied together with phosphate buffered solution. For equal ethanol concentrations, no difference was observed between the dilution in PBS or water; this is because water and PBS have very similar values of density and viscosity.

Concerning the behavior of the two laminar flows (PBS–ethanol [X%]), as the ethanol concentration was higher, the difference between density and viscosity of both fluids was larger (ethanol has lower density but higher viscosity), requiring a higher flow rate through the PBS inlet for a given chamber occupation. In addition, there was also higher diffusion. For illustration, in the lines below we explain the flow rate ratio required to obtain a 50% chamber occupation for different ethanol concentrations (Fig. 4). In this case, the ratio between inlets ($Q_{PBS}/Q_{ethanol}$) instead of being 1 should be approximately 2.4 for ethanol at 25%, or almost 3 for ethanol at 50%.

As shown, the use of control curves based on ratios makes the calibration scalable to different flow rate ranges; the use of lower or higher flows will depend on the particular assay requirements. These curves make the control of the device very simple and fully

customizable since taking all these phenomena into consideration for each specific assay or study may be complicated and time consuming. Nevertheless, if the density or the viscosity were too different the control curves could be readjusted, and since we have also developed home-made MATLAB-based interface detection software this work would be done semi-automatically.

3.3. Cell trapping protocol optimization

Loading time, flow velocity and cell density are the most important parameters when optimizing cell trapping without affecting cell viability. We found that cells should be loaded within 5–10 min after starting the perfusion of the cell suspension. This helps to minimize the amount of shear stress exerted on cells during the trapping stage.

Pumping cells at high flow rates leads to a faster trapping step and to a minimized loading time. However, cells could suffer excessive shear stress under these conditions, which could compromise cell behavior and the integrity of the membrane, resulting in cell death (Kobel et al., 2010; Li et al., 2005). Most endothelial cells could withstand up to 10 μL/min flow rates, which are similar to interstitial flow velocities found within the human body (Helm et al., 2005; Polacheck et al., 2013; Swartz and Fleury, 2007). In contrast, if the loading velocity is too low the underlying mechanism of trapping, based on the hydrodynamic resistance of the traps, would not work properly since the cells would dodge the sieves. A flow rate of 1–3 μL/min maximized both viability and trapping efficiency. In addition, cell density also played a crucial role in the trapping dynamics. Increasing cell density leads to shorter loading times. We found that the optimal density was $3.0–5.0 \times 10^5$ cells/mL. Higher densities lead to clogging of the microchannels and multiple cells lodging per trap.

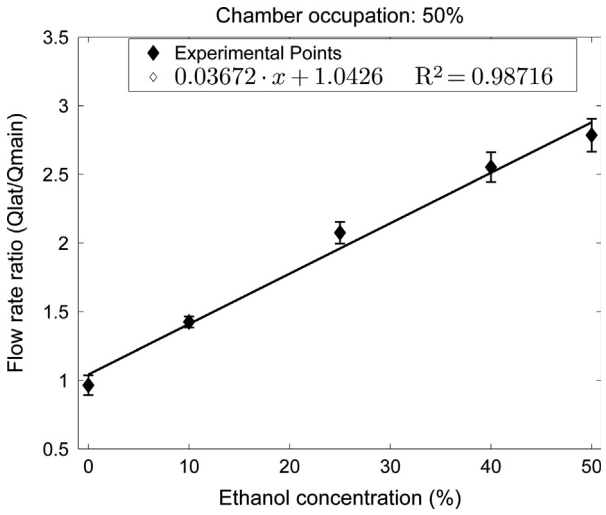

Fig. 4. Flow rate ratio between the lateral inlet (Q_{lat}) over the main inlet (Q_{main}) for a chamber occupation of 50% and for different ethanol concentrations. The mean values for concentrations equal to 0%, 10%, 25%, 40% and 50% are .97, 1.43, 2.08, 2.55, 2.79, 2.76 and 2.11. Obtained standard deviations are .07, .04, .08, .11 and .12 for 0%, 10%, 25%, 40% and 50% ethanol concentrations respectively.

Cell trapping efficiency of the device was evaluated optically. Traps filled with impurities or with faulty pillars were not taken into account. Cell perfusion was done just for 5–10 min. In total, six different devices were evaluated obtaining an average efficiency of 81.6% (SEM ± 3.1; SD ± 7.5). These acquired values are comparable to those found in the literature with high efficiency rates and based on similar hydrodynamic traps (Hong et al., 2012; Lin et al., 2013; Xu et al., 2013). Hence, the arrangement and shape of these elements appears to be adequate. However, no difference was observed among the three used geometries of the traps. Therefore, we conclude that once the gap of the trapping structures is properly selected (6 μm in this work), the shape of the trap itself is not crucial as long as the space that accommodates the cell has a similar size to the dimensions of the cell under study.

3.4. Cytotoxicity assay

Using this microfluidic platform and the developed control curves (Figs. 3b and 4), we can selectively treat single cells simultaneously and under the same conditions by simply adjusting the flow rate ratio between the inlets. In order to further validate the device, we evaluated the cytotoxic effect of ethanol at different concentrations, from 10 to 50%, on isolated hepatocytes.

For each ethanol concentration, the procedure presented below was carried out. In particular, Fig. 5 illustrates the process when ethanol concentration was fixed to 25%. Following the cell trapping step (see Fig. 5a and b), described in the Materials and

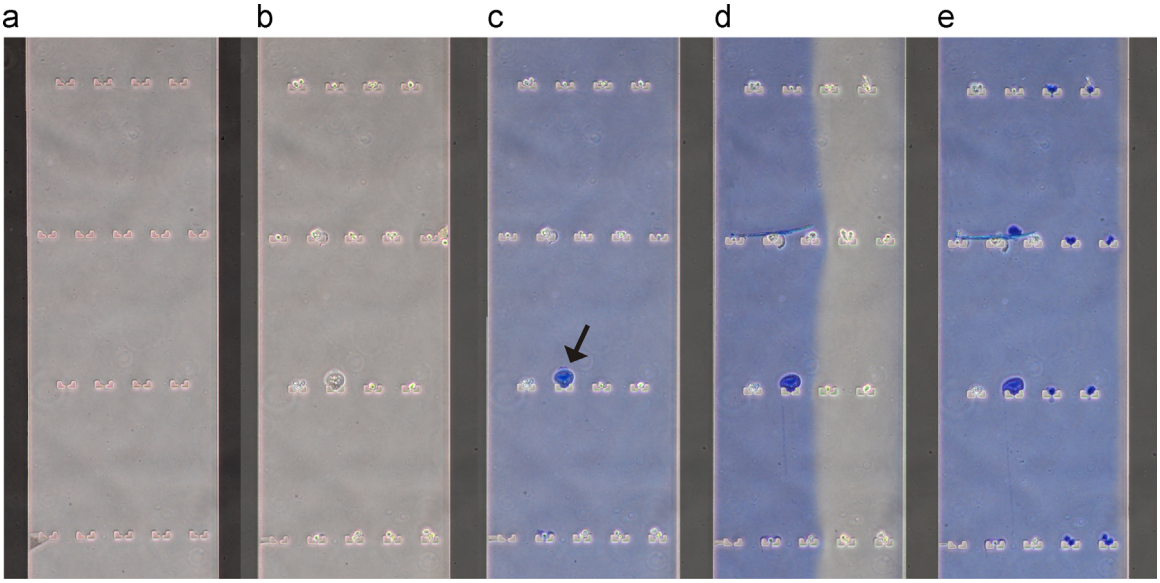

Fig. 5. Cytotoxicity assay for ethanol at 25%. (a) Empty chamber flushed with PBS and with no stacked air bubble. (b) Trapped single cells after 5 min. (c) Trypan blue exclusion test; note that one cell is already dead. (d) Ethanol treatment to 50% of the cells. (e) Cell viability checking after the treatment. An extra figure showing a particular trapped cell, at higher magnification before and after the treatment, can be found in the supporting information (see Fig. S5).

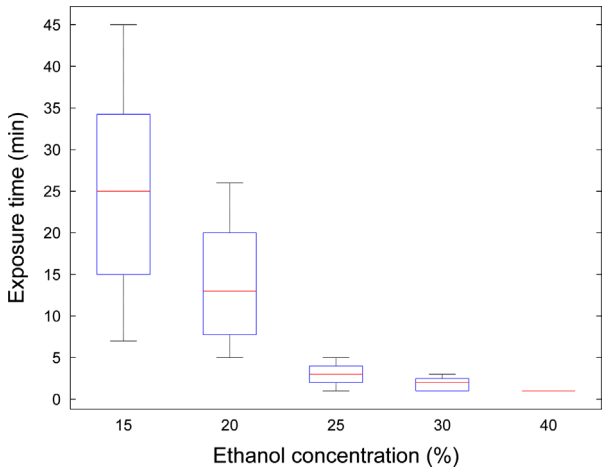

Fig. 6. Exposure time until cell death at different ethanol concentrations. At concentrations higher than 40% cells die in few seconds. Whereas, if the ethanol percentage is 10% or lower the cytotoxic effect is minimum requiring an exposure longer than 60 min. More detailed data is included in the Table S1 of the supporting information.

methods section, the device was ready to carry out the cytotoxicity assay. The ethanol was driven through the main inlet while the trypan blue was injected through the lateral inlet. The input flow rate ratio was fixed so as to treat selected cells by halting the ethanol controlling syringe pump at determined periods (every minute during the first 5 and then every 5 min until every cell was dead) to identify death cells by trypan blue exclusion test (Fig. 5c).

In order to facilitate the understanding of the whole purpose of this work we demonstrated its operation with a fixed chamber occupation of a 50%, that is, half of the isolated cells were treated with ethanol whereas the other half worked as control (see Fig. 5d). Fig. 5e shows how cells treated with 25% ethanol died within 5 min. Data in Fig. 3b can be easily adapted to obtain the specific ratios to control the flow through any device fulfilling the conditions previously described. Regarding this particular microfluidic platform, note that the traps barely modify the flow through the chamber. In addition, as posed above, the flow can be considered fully developed once it reaches the chamber (see Fig. S4).

Recalling this particular case for treating half of the isolated cells, we identified that the proper ratio needed for a 50% of chamber occupation was $Q_{lat}/Q_{main}=2.4$ (Fig. 4). Once the specific ratio was known, the ethanol (Q_{main}) and the PBS (Q_{lat}) inlet flow rates were always fixed to values as close to 5 μL/min as possible, such as $Q_{lat}=7.13$ μL/min and $Q_{main}=3$ μL/min; proper values both assuring cell viability (never higher than 10 μL/min, shear stress would compromise the cell membrane integrity) and, as commented above, with negligible diffusion at the interface of both fluids (not lower than 1 μL/min).

Fig. 6 shows the time until cell death for each ethanol concentration. The cytotoxicity increased with ethanol dosage and with exposure time. As the ethanol concentration increases, the time to cell death decreases rapidly. Hepatocytes exposed to 40% and 50% ethanol died in less than 1 min, these resulting in the highest doses to which they were subjected. At 30% of ethanol, all cells were dead within the first 3 min, whereas cells under 25% ethanol treatment died after almost 5 min. On the other hand, at lower ethanol concentrations cells withstand better the exposure. The longer the contact to ethanol, the more differences cell to cell were observed. When treating cells with 20% ethanol, we found that some cells died after 10 min whereas other survived even 15 more minutes. Similarly, at 15% ethanol the first cells died in 20 min but it took a total of 35 min until 80% of the cells were dead. These were expected results due to the heterogeneity of each individual cell, for instance, apart from the ethanol effect not all the cells are in the same stage of the cell cycle. A concentration as low as 10% entailed much more than 60 min to affect all the cells. After 60 min the ethanol infusion was stopped to avoid misleading results considering that for longer assays other factors disturbing cell viability, such as CO_2 absence or temperature changes, should be taken into account. It is worth noting that the averaged acquired exposure times as a function of ethanol concentration, were coherent as shown in Fig. 6. In addition, these results of ethanol cytotoxicity in hepatocytes are in line with previously reported ones by Tapani et al. (1996) on conventional culture plates and they provide with more quantitative information (see Supplementary Table S1). In our study, cells exhibited higher resistance to ethanol exposure than in the experiment performed by Tapani and coworkers. These differences are probably due to two main reasons: a perfusion culture compared with a static culture (Wu et al., 2010) and an averaged cytotoxicity data from a cell population versus results at individual cell level. This emphasized again the versatility of this microfluidic platform that enables perfusion cultures which not only have steadier and more controllable conditions but also provide the ability of acquiring single-cell data.

4. Conclusion

This paper presents a microfluidic platform for single cell trapping and selecting probing under different conditions. Predictable laminar flow allows the acquisition of control curves for selective on-chip treatment of cells in a versatile and simple manner. Proof-of-concept experiments were conducted using a single-cell ethanol cytotoxicity assay. We demonstrate that for small number/scarce cell populations, as is appropriate for patient-derived rare cancerous cells, we can produce statistically robust information collecting data from individual cells. The versatility of this microfluidic platform makes it a powerful tool for performing different single cell-based assays of high interest in cell-based drug testing, cancer research or cell therapy. The device herein described could also be of relevance for applications in multifunctional cell-based biosensors (Asphahani et al., 2008; Thein et al., 2010; Xu et al., 2005). As such, trapped cells serving as sensing elements could allow for monitoring of physiological changes induced by the exposure to different environmental stimuli.

Acknowledgments

The authors are grateful to Jon Pey for his helpful discussions and Matlab programming assistance. The authors acknowledge the Basque Government for the grant promoting doctoral theses for young pre-doctoral researchers (BFI-2010-236) and the Secretary of State of Investigation, Development and Innovation of the Ministry of Economy and Competitivity of Spain for funding this research within the framework of the SIMcell Project DPI 2012-38090-C03-D3.

Appendix A. Supplementary Information

Supplementary data associated with this article can be found in the online version at http://dx.doi.org/10.1016/j.bios.2014.05.036.

References

Arakawa, T., Noguchi, M., Sumitomo, K., Yamaguchi, Y., Shoji, S., 2011. Biomicrofluidics 5, 014114.
Asphahani, F., Thein, M., Veiseh, O., Edmondson, D., Kosai, R., Veiseh, M., Xu, J., Zhang, M., 2008. Biosens. Bioelectron. 23 (8), 1307–1313.
Bange, A., Halsall, H.B., Heineman, W.R., 2005. Biosens. Bioelectron. 20 (12), 2488–2503.
Benavente-Babace, A., Gallego-Pérez, D., Hansford, D., Arana, S., Pérez-Lorenzo, E., Mujika, M., 2013. XIII Mediterranean Conference on Medical and Biological Engineering and Computing 2013. Springer International Publishing, 2014, Seville, Spain, pp. 864–867.
Bhagat, A.A., Kuntaegowdanahalli, S.S., Kaval, N., Seliskar, C.J., Papautsky, I., 2010. Biomed. Microdevice 12 (2), 187–195.
Chou, J., Du, N., Ou, T., Floriano, P.N., Christodoulides, N., McDevitt, J.T., 2013. Biosens. Bioelectron. 42, 653–660.
Di Carlo, D., Lee, L.P., 2006. Anal. Chem. 78 (23), 7918–7925.
Faley, S.L., Copland, M., Wlodkowic, D., Kolch, W., Seale, K.T., Wikswo, J.P., Cooper, J.M., 2009. Lab Chip 9 (18), 2659–2664.
Frimat, J.-P., Becker, M., Chiang, Y.-Y., Marggraf, U., Janasek, D., Hengstler, J.G., West, J., 2011. Lab Chip 11 (2), 231–237.
Graf, T., Stadtfeld, M., 2008. Cell Stem Cell 3 (5), 480–483.
Helm, C.L., Fleury, M.E., Zisch, A.H., Boschetti, F., Swartz, M.A., 2005. Proc. Natl. Acad. Sci. USA 102 (44), 15779–15784.
Hong, S., Pan, Q., Lee, L.P., 2012. Integr. Biol. 4 (4), 374–380.
Hur, S.C., Tse, H.T.K., Carlo, D.D, 2010. Lab Chip 10 (3), 274–280.
Jeon, N.L., Dertinger, S.K., Chiu, D.T., Choi, I.S., Stroock, A.D., Whitesides, G.M., 2000. Langmuir 16 (22), 8311–8316.
Joo, S., Kim, K.H., Kim, H.C., Chung, T.D., 2010. Biosens. Bioelectron. 25, 1509–1515.
Kobel, S., Valero, A., Latt, J., Renaud, P., Lutolf, M., 2010. Lab Chip 10 (7), 857–863.
Kovacs, G.T., 1998. Micromachined Transducers Sourcebook. WCB/McGraw-Hill, New York.
Li, L., Nie, Y., Shi, X., Wu, H., Ye, D., Chen, H., 2011. Biomicrofluidics 5 (3), 036503.
Li, S., Huang, N.F., Hsu, S., 2005. J. Cell. Biochem. 96 (6), 1110–1126.
Lin, L., Chu, Y.-S., Thiery, J.P., Lim, C.T., Rodriguez, I., 2013. Lab Chip 13 (4), 714–721.
Oakey, J., Applegate, R.W., Arellano, E., Carlo, D.D., Graves, S.W., Toner, M, 2010. Anal. Chem. 82 (9), 3862–3867.
Parra-Cabrera, C., Sporer, C., Rodriguez-Villareal, I., Rodriguez-Trujíllo, R., Homs-Corbera, A., Samitier, J., 2012. Lab Chip 12 (20), 4143–4150.
Polacheck, W.J., Li, R., Uzel, S.G., Kamm, R.D., 2013. Lab Chip 13 (12), 2252–2267.
Rowat, A.C., Bird, J.C., Agresti, J.J., Rando, O.J., Weitz, D.A., 2009. Proc. Natl. Acad. Sci. USA 106 (43), 18149–18154.
Sia, S.K., Whitesides, G.M., 2003. Electrophoresis 24 (21), 3563–3576.
Skommer, J., Akagi, J., Takeda, K., Fujimura, Y., Khoshmanesh, K., Wlodkowic, D., 2012. Biosens. Bioelectron. 42, 586–591.
Stroock, A.D., Dertinger, S.K., Ajdari, A., Mezić, I., Stone, H.A., Whitesides, G.M., 2002. Science 295 (5555), 647–651.
Swartz, M.A., Fleury, M.E., 2007. Annu. Rev. Biomed. Eng. 9, 229–256.
Takayama, S., McDonald, J.C., Ostuni, E., Liang, M.N., Kenis, P.J., Ismagilov, R.F., Whitesides, G.M., 1999. Proc. Natl. Acad. Sci. USA 96 (10), 5545–5548.
Takayama, S., Ostuni, E., LeDuc, P., Naruse, K., Ingber, D.E., Whitesides, G.M., 2001. Nature 411 (6841), 1016.
Tapani, E., Taavitsainen, M., Lindros, K., Vehmas, T., Lehtonen, E., 1996. Acta Radiol. 37 (6), 923–926.
Thein, M.A., Cheng, A., Buckmaster, R., Zhang, M., Xu, J., 2010. Biosens. Bioelectron. 25, 1963–1969.
Toner, M., Irimia, D., 2005. Annu. Rev. Biomed. Eng. 7, 77–103.
Velve-Casquillas, G., Le Berre, M., Piel, M., Tran, P.T., 2010. Nano Today 5 (1), 28–47.
Walling, M., Shepard, J., 2011. Chem Soc. Rev. 40, 4049–4076.
Wang, Z.-H., Takada, N., Uno, H., Ishizuka, T., Yawo, H., Urisu, T., 2012. Colloids Surf. B 96, 44–489.
Wang, T., Hu, N., Cao, J., Su, K., Wu, J., Wang, P., 2013. Biosens. Bioelectron. 49, 9–13.
Weigl, B., Domingo, G., LaBarre, P., Gerlach, J., 2008. Lab Chip 8 (12), 1999–2014.
Wu, L.Y., Di Carlo, D., Lee, L.P., 2008. Biomed. Microdevices 10 (2), 197–202.
Wu, M.-H., Huang, S.-B., Lee, G.-B., 2010. Lab Chip 10 (8), 939–956.
Xu, G., Ye, X., Qin, L., Xu, Y., Li, Y., Li, R., Wang, P., 2005. Biosens. Bioelectron. 20, 1757–1763.
Xu, X., Sarder, P., Li, Z., Nehorai, A., 2013. Biomicrofluidics 7, 014112.
Zare, R.N., Kim, S., 2010. Ann. Rev. Biomed. Eng. 12, 187–201.